Mechanical Systems and Signal Processing 225 (2025) 112271

Contents lists available at ScienceDirect

Mechanical Systems and Signal Processing

journal homepage: www.elsevier.com/locate/ymssp

Invited for the Special Issue in Honor of Professor John Mottershead

Position optimization of Stockbridge dampers under varying operating conditions: A comprehensive finite element and experimental analysis

Erdi Gulbahce [a,b], Sunit K. Gupta [b], Oumar Barry [b,*]

[a] Department of Mechatronics Engineering, KTO Karatay University, Konya, Turkey
[b] Department of Mechanical Engineering, Virginia Polytechnic Institute and State University, Blacksburg, VA 24061 USA

ARTICLE INFO

Keywords:
Aeolian vibrations
Power line
Stockbridge damper
Burst random
Finite element analysis

ABSTRACT

The placement of a Stockbridge damper within a powerline conductor is critical for its effectiveness in mitigating aeolian vibrations. This paper investigates the optimal positioning of Stockbridge dampers under varying operating conditions using the finite element method (FEM), incorporating both modal and harmonic response analyses. We compare the performance of two commercially available Stockbridge dampers, symmetrical and asymmetrical models, using FEM to obtain the normalized optimal placement for both dampers on the conductor. The results show that the asymmetrical damper, when placed at its optimal location, provides superior vibration suppression compared to the symmetrical model at its optimal location and both dampers when placed at conventional positions. In a novel approach, an experimental investigation is conducted on the commercial asymmetrical damper to refine its finite element model and determine its optimized placement. The experimental study employs both burst random and sine-sweep tests, with the burst random test proving to be more accurate and consistent in identifying the damper's natural frequencies and mode shapes. This study is the first to demonstrate the effectiveness of the burst random test in the context of Stockbridge dampers. Finally, we use the experimentally validated finite element model to determine the optimized placement of the asymmetrical damper on a real-life powerline conductor, achieving significantly improved vibration mitigation. These findings offer valuable insights for improving the performance and longevity of powerline systems.

1. Introduction

Wind-induced vibrations are a major cause of excessive oscillations of transmission lines/conductors, eventually leading to their failure [1–5]. These vibrations in transmission lines can be classified into three primary types: 1) galloping, 2) wake-induced oscillations, and 3) aeolian vibrations [6,7]. Galloping is characterized by low-frequency oscillations from 0.1 to 1 Hz on power lines, caused by asymmetric ice formation, altering the aerodynamic profile of power lines, and generating destabilizing lift forces. These vibrations can reach the amplitudes of approximately up to 20 to 300 times the diameter of the transmission line, potentially causing severe damage to transmission line integrity [7]. Wake-induced vibrations of transmission lines typically occur as alternating

* Corresponding author.
E-mail address: obarry@vt.edu (O. Barry).

https://doi.org/10.1016/j.ymssp.2024.112271
Received 17 July 2024; Received in revised form 28 October 2024; Accepted 21 December 2024
Available online 27 December 2024

aerodynamic forces arise from the wake of airflow. These vibrations happen within a medium-frequency range of up to 10 Hz and exhibit displacement amplitudes up to 1 m under steady wind conditions [7,8]. On the other hand, aeolian vibrations, caused by steady winds passing through power lines, lead to small but rapid oscillations as vortices shed at frequencies matching the natural frequencies of the cables. These vibrations typically range from 3-150 Hz with amplitudes less than one cable diameter [9]. While the fundamental aerodynamic mechanisms of galloping due to wind-induced vibrations are well-understood, predicting the exact conditions under which galloping occurs remains challenging due to the complex interplay of environmental factors and conductor characteristics. Instead, due to their frequent occurrence and potential for causing instability, aeolian vibrations have been a major focus of research. These vibrations can lead to catastrophic accidents, resulting in injuries, fatalities, and substantial economic losses [10]. Therefore, in this work, we focus on the optimized means of suppressing the aeolian vibrations of the conductor and mitigating their detrimental effects.

The use of vibration absorbers to minimize aeolian vibrations is well-established in the literature. These vibration absorbers can be classified into three types: passive, active, and semi-active [11,12]. It should be noted that passive vibration absorbers in the form of tuned vibration absorbers are more prevalent than active and semi-active ones due to their simplicity, ease of installation, and durability [11,13,14]. As passive vibration absorbers, Stockbridge dampers are utilized to mitigate aeolian vibrations in transmission lines [8,15,16]. Note that the performance of a Stockbridge damper depends on its ability to exhibit multiple tunable frequencies and its optimal placement along the conductor. The asymmetrical Stockbridge damper dynamically adjusts the damping force in response to varying excitation frequencies, owing to having more resonance modes. This leads to a more effective reduction of vibration amplitudes compared to symmetrical counterparts. The next crucial factor is the optimum location of the damper. Traditionally, the ideal location for a Stockbridge damper is at the antinode of the vibration mode [8,17–20]. However, the mode shape of the conductor changes with varying wind velocities, making it challenging to ensure that the damper is always located at the antinode for every mode. Due to the dynamic nature of aeolian vibrations, the mode shape of the conductor continuously changes, which can potentially amplify the vibrations if they resonate with the conductor's natural frequencies.

To overcome the challenges mentioned above associated with the Stockbridge damper, Barry et al. [9,21] developed a mobile damping robot (MDR). Since the MDR adapts to the wind characteristics and relocates itself to the antinode of the corresponding mode, the MDR has been proven to be more advantageous than the Stockbridge damper [9,21]. However, as the MDR navigates along the conductor, the nodes and antinodes change, affecting the conductor's dynamics and mode shapes. Therefore, to determine the optimum location of the MDR for better vibration mitigation, it is necessary to conduct the frequency response analysis of the conductor as the MDR moves along the span. This is the prime focus of the current work. By identifying the optimal locations for the Stockbridge damper under various controlled conditions, we lay the groundwork for developing algorithms that enable the MDR to dynamically adjust its position in real-time, thereby maintaining optimal damping efficacy regardless of changing environmental conditions. Note that the single degree of lumped parameter model of the Stockbridge damper has been analyzed numerically in the literature [20]. However, in real-life applications, the Stockbridge damper exhibits more than one degree of freedom, making it challenging to analyze the entire system of conductors with the damper numerically.

The shortcomings of the numerical methods can be overcome using finite element-based software since it can be easily applied to the entire conductor model with the Stockbridge damper. The optimum location of the conductor for different operating conditions can be found more effectively using vibration analysis. Therefore, in this work, we use finite element analysis (FEA) to determine the frequency responses of the conductor along with the Stockbridge damper at different locations and obtain the optimal location for the damper under varying operating conditions. It should be noted that the effectiveness of FEA can be further enhanced by incorporating an experimentally verified Stockbridge damper finite element (FE) model and can be helpful in determining the optimal location of the commercially available Stockbridge damper.

Experimental methods, such as sine-sweep tests and burst random tests, can be employed to identify mode frequencies and critical vibration modes [22–25]. However, we emphasize that, to the author's best knowledge, burst random tests have not been employed in the case of the Stockbridge damper and, hence, to define the modal parameters. This paper, for the first time, uses the burst random test to define the model parameters for the case of the Stockbridge damper. We observe that the burst random test is more effective than the sine-sweep test in the case of the Stockbridge dampers. Subsequently, a new FE model is utilized to determine the optimal location for a real Stockbridge damper.

The rest of the paper is organized as follows. In Section 2, we present the system description along with the Ansys model. Numerical simulations involving the validation of the Ansys model and optimum locations of symmetrical and asymmetrical dampers are

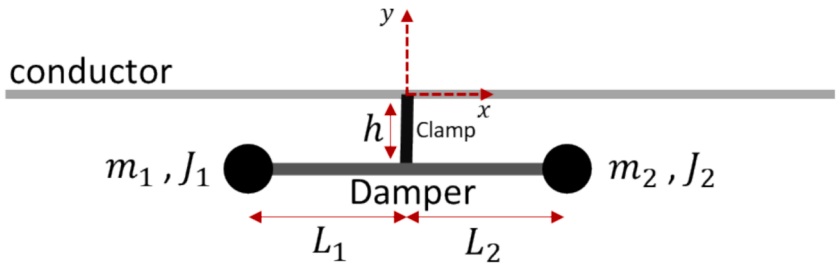

Fig. 1. Schematical power line conductor and damper.

presented in Section 3. In Section 4, we present the experimentally verified Ansys model of a commercial damper along with the optimal location using vibration analysis. Finally, conclusions are drawn in Section 5.

2. System description and modeling in ANSYS

In this section, we present the finite element (FE) modeling of the conductor along with the Stockbridge damper using ANSYS Workbench 2022-R1. The schematic of the conductor and damper model is shown in Fig. 1. It is important to note that modeling a power line conductor poses significant challenges due to its intricate structure, which comprises closely arranged individual round wires in counter-rotating helices. Therefore, for the finite element analysis (FEA), we adopt a simplified solid cylindrical body with a homogeneous structure throughout the cross-sectional area and length of the conductor [26].

In the current analysis, we use two available models of Stockbridge dampers: symmetrical and asymmetrical. If the counterweights (m_1, m_2) or the messenger lengths (L_1, L_2) in the Stockbridge dampers are not equal, then the damper is considered asymmetrical; otherwise, it is symmetrical. The conductor is made of Aluminum, while the messenger in the Stockbridge damper is made of Steel. Table 1 summarizes the properties of the conductor, symmetrical damper, and asymmetrical damper.

We model the conductor and the damper in ANSYS using BEAM188 [27], which utilizes Timoshenko beam theory and is more suitable for the conductor [10]. In contrast, the two counterweights at the end of the damper messengers are modeled as three-dimensional lumped masses. The rotational moments of inertia are included in the lumped masses to account for the dynamics of the Stockbridge dampers [28]. Furthermore, the clamp between the damper and conductor is modeled as a stiff beam, and the damper model is attached to the cable using a fixed joint. To reduce computation time, line bodies are utilized for conductors and dampers. Fig. 2 depicts the FE model of the conductor with a damper.

For the analysis in ANSYS, we use 775 elements in the damper and conductor and employ the default solver to perform the analysis. The free vibration analysis of the bare conductor is conducted through the modal analysis toolbox in ANSYS, utilizing supported boundary conditions on both ends of the span. These conditions are achieved by restricting the displacements along the x-axis and y-axis while permitting the rotation around the z-axis to satisfy the Euler-Bernoulli beam theory.

3. Modal analysis

After establishing the ANSYS model of the conductor with the Stockbridge damper, we perform a modal analysis of the system. However, before proceeding further, it is essential to validate the FE model of the conductor and absorber, as presented in the next section.

3.1. Validation of the FE model

To validate our current FE model of the Stockbridge damper, we compare it against the model analyzed by Barry et al. [19]. For this, we focus on the free linear vibration analysis of the absorber, and compare it with the linear analyses presented in [19]. Therefore, we utilize line elements to perform the FEA of the conductor. Furthermore, Barry et al. [19] investigated three cases of Stockbridge dampers: one symmetrical and two asymmetrical, each with different geometric and mechanical properties. For completeness, we compare our FE model of the absorber with the three corresponding cases reported in [19]. This further allows us to validate the current model more efficiently. The comparison between the current FE model and the reference study is summarized in Table 2.

From Table 2, we observe a good agreement between the current FE model of the damper and the model reported in [19]. The maximum relative error observed in the analysis is 2.0712 %, indicating a high level of accuracy. Therefore, we use the proposed FE model of the Stockbridge absorber for further analysis.

In the subsequent analysis, we conduct the free vibration analysis of both symmetric and asymmetric dampers with properties listed in Table 1. For both cases of the damper, the FE model is fixed to the ground at the clamp, and the clamp and damper messengers are connected via a fixed joint. The mode shapes for both models are depicted in Fig. 3 to visually distinguish the dynamical characteristics of symmetric and asymmetric dampers. Furthermore, the natural frequencies of the symmetrical and asymmetrical damper for different modes are listed in Table 3.

Table 1
Parameters of the conductor and dampers.

	Conductor	***Sym. Damper***	***Asym. Damper***
Diameter (mm)	14.4	3	3
Lenght (m)	7.32	$L_1 = L_2 = 0.2$	$L_1 = 0.2, L_2 = 0.26$
Rotational moment of inertia $(kg.mm^2)$	–	$J_1 = J_2 = 300$	$J_1 = 300, J_2 = 500$
Height of the clamp (mm)	–	$h = 20$	$h = 20$
Elasticity (GPa)	71	200	200
Poisson's ratio	0.33	0.3	0.3
Mass density (kg/m^3)	2148	5575	5575
Counter weight (kg)	–	$m_1 = m_2 = 0.3$	$m_1 = 0.3, m_2 = 0.5$
Mass per length (kg/m)	0.3493	0.25	0.25
Tension (N)	872	–	–

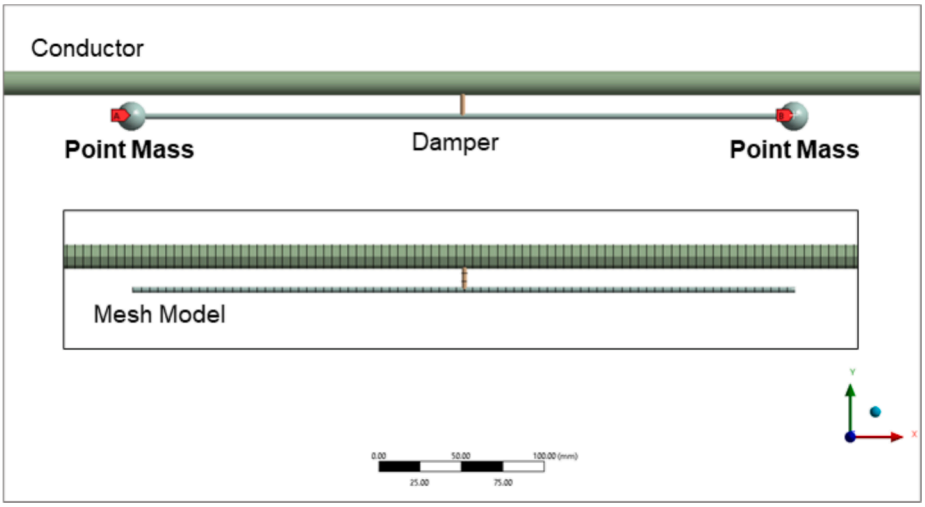

Fig. 2. FE model of the symmetrical damper with conductor.

Table 2
The natural frequencies of the validation study (in Hz).

	Damper 1(Symmetrical)		*Damper 2 (Asymmetrical)*		*Damper 3 (Asymmetrical)*	
Modes	*Our Model*	*Reference Model* [19]	*Our Model*	*Reference Model* [19]	*Our Model*	*Reference Model* [19]
1st	*6.77*	*6.70*	*5.57*	*5.64*	*13.53*	*13.81*
2nd	*31.10*	*30.80*	*13.02*	*13.17*	*25.23*	*25.76*
3rd	–	–	*30.71*	*31.07*	*51.16*	*52.02*
4th	–	–	*52.24*	*52.90*	*96.05*	*97.04*

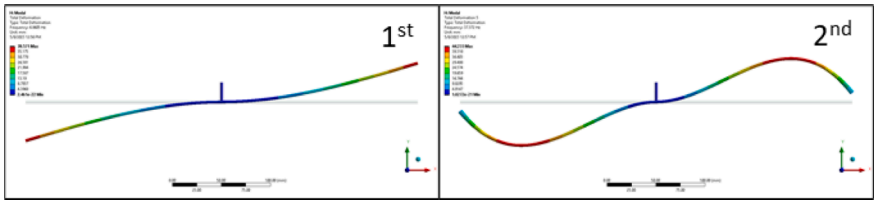

(a)

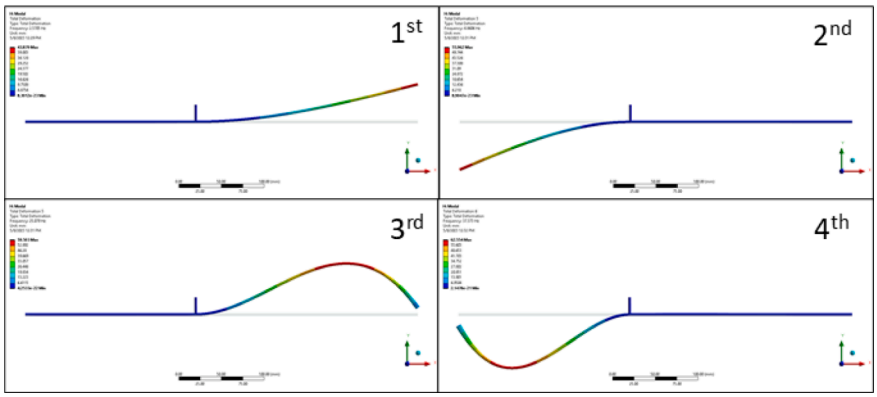

(b)

Fig. 3. The mode shapes (a) symmetrical damper, (b) asymmetrical damper.

In the next step, we validate our FE model of the conductor by comparing the free vibration analysis of the FE model, analytical model, and experimental results. Specifically, we compare the linear natural frequencies obtained using three methodologies. The analytical natural frequency of the bare conductor can be obtained using the Euler-Bernoulli beam theory and is given by [26,29,30].

$$\omega_n = \frac{n}{2L}\sqrt{\frac{T}{\rho A} + \left(\frac{n\pi}{L}\right)^2 \frac{EI}{\rho A}} \tag{1}$$

In Eq. (1), n is an integer indicating the mode number ($n = 1, 2, \ldots$), L is the length of the power line conductor, T is the pretension, ρA is the mass per unit length, and EI is the flexural rigidity.

The free vibration analysis of the FE model of the bare conductor is conducted through the modal analysis toolbox in Ansys, utilizing simply supported boundary conditions at each end. As mentioned earlier, these boundary conditions are obtained by restricting the displacement of the conductor along the x and y-axis while allowing the rotation about the z-axis. To obtain the natural frequencies of the bare conductor, a pre-stressed modal analysis is performed, followed by a static structural analysis. For this, we use an APDL command that applies a pretension of 872 N and is consistent with our experimental setup. Next, the experimental modal frequencies of the bare conductor are obtained via a hammer test. Table 4 compares the bare conductor's analytical, numerical, and experimental natural frequencies. From Table 2, we can observe a good agreement between the FE model with analytical and experimental results. This agreement further validates the effectiveness of our FE model of the bare conductor, which will be used for the remaining analysis.

3.2. Frequency response analysis of the conductor with damper

The harmonic response analysis is a valuable technique for validating the structural design and its ability to handle resonance failures [31–33]. Therefore, in our study, we use the harmonic response analysis toolbox available in ANSYS to evaluate the response of a structure subjected to sinusoidal dynamic loading. We emphasize that simulating precise wind velocities responsible for aeolian vibrations in powerlines can be challenging due to the complexity of replicating real-world environmental conditions in FEA. Therefore, instead of directly modeling specific wind velocities causing aeolian vibrations, we opted to focus on the dynamic behavior of the conductor within a frequency range of 0–150 Hz (with intervals of 0.5 Hz), which effectively captures the typical range for aeolian vibrations. This approach enables us to analyze the system's response to various excitation frequencies without needing to simulate specific wind speeds. Additionally, to account for varying wind velocities and excitation amplitudes, we performed the analysis using a force amplitude range of 1 N to 10 N, applied along the conductor's y-axis.

Similar to the free vibration analysis, the boundary conditions for the modal analysis are set to be simply supported at both ends. To avoid unrealistically high responses at resonance frequencies, a small constant damping ratio (0.02) is added to the analysis. Finally, the mode superposition method is employed to determine the modal parameters, including natural frequencies and mode shapes of the system, which are then used to characterize the harmonic response analysis.

As mentioned earlier, as MDR moves along the length of the conductor, it changes the nodes and antinodes of different modes and hence, the resulting optimum location. Therefore, it is essential to determine the change in the dynamics of the conductor with different locations of MDR and, in the current case, the Stockbridge damper. Since we are using the simply supported boundary conditions at each end and only one Stockbridge damper, the system exhibits symmetry about the midpoint of the conductor. Hence, to simplify the analysis, we focus on half of the conductor's length. Accordingly, one-half of the conductor (approximately 3.6 m) is divided into 18 equal segments of 0.2 m. The Stockbridge damper is attached to these 18 equidistant points, and the harmonic response analysis is conducted for each case in the frequency range of 0–150 Hz. The 'USUM' command in ANSYS is used to measure the system's displacement response, providing the conductor's maximum deformation for a given frequency. Since analyzing the system for a specific frequency is not an optimal approach, we obtain the displacement response of the system for the frequency range of 0–150 Hz. However, we only present the analysis within 0–50 Hz to better understand these results.

Fig. 4 depicts the root mean square (RMS) values of the displacement response of the conductor for different damper locations within the 0–50 Hz frequency range. The x-axis represents the normalized location of the damper $\left(\frac{x}{L}\right)$ with respect to the length of the conductor L. On the other hand, the y-axis represents the normalized maximum displacement $\left(\frac{y}{d}\right)$ of the conductor with respect to the diameter of the conductor's cross-section d. This normalization allows comparison of performance irrespective of the physical dimensions of different conductors or dampers. Furthermore, Fig. 4 provides insight into the optimal location of the damper to minimize the vibrations of the conductor for the given frequency range. In this analysis, the damper's optimal location implies the position of the damper corresponding to the lowest maximum vibration amplitude across the frequency range of 0–50 Hz. With this objective

Table 3
The natural frequencies and the direction of the mode shapes.

Modes	*Symmetrical Damper [Hz]*	*Asymmetrical Damper [Hz]*	*Mode Shapes*
1st	*4.86*	*2.57*	*y-axis bending*
2nd	*37.37*	*4.86*	*y-axis bending*
3rd	–	*25.08*	*y-axis bending*
4th	–	*37.37*	*y-axis bending*

Table 4
Analytical, numerical, and experimental natural frequencies of the bare conductor.

Modes	*Analytical (Beam) [Hz]*	*ANSYS (Beam) [Hz]*	*Experimental [Hz]*
1st	*3.46*	*3.46*	*3.88*
2nd	*7.24*	*7.24*	*7.40*
3rd	*11.60*	*11.60*	*11.5*
4th	*16.75*	*16.75*	*15.5*

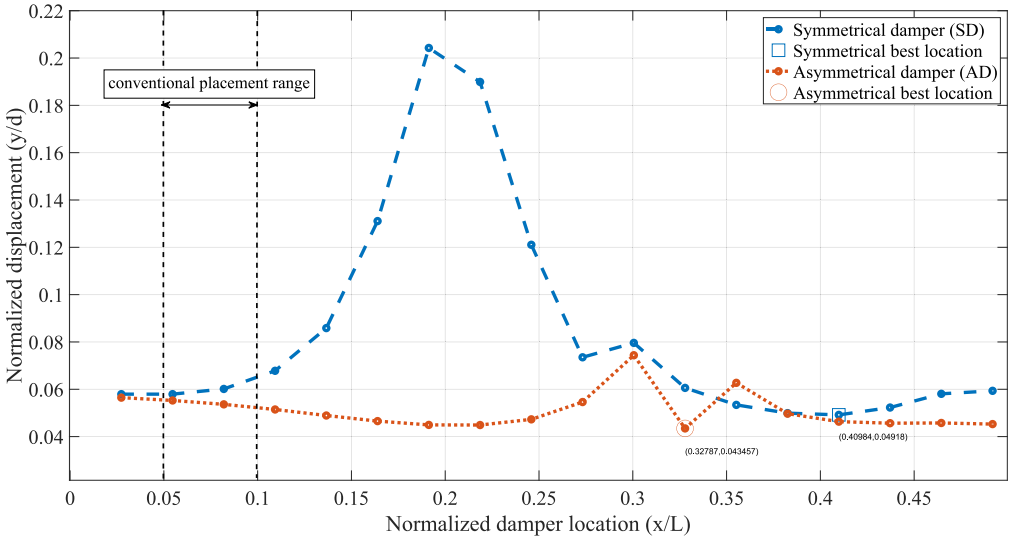

Fig. 4. The root mean square (RMS) of the displacement responses for the normalized location (0–50 Hz).

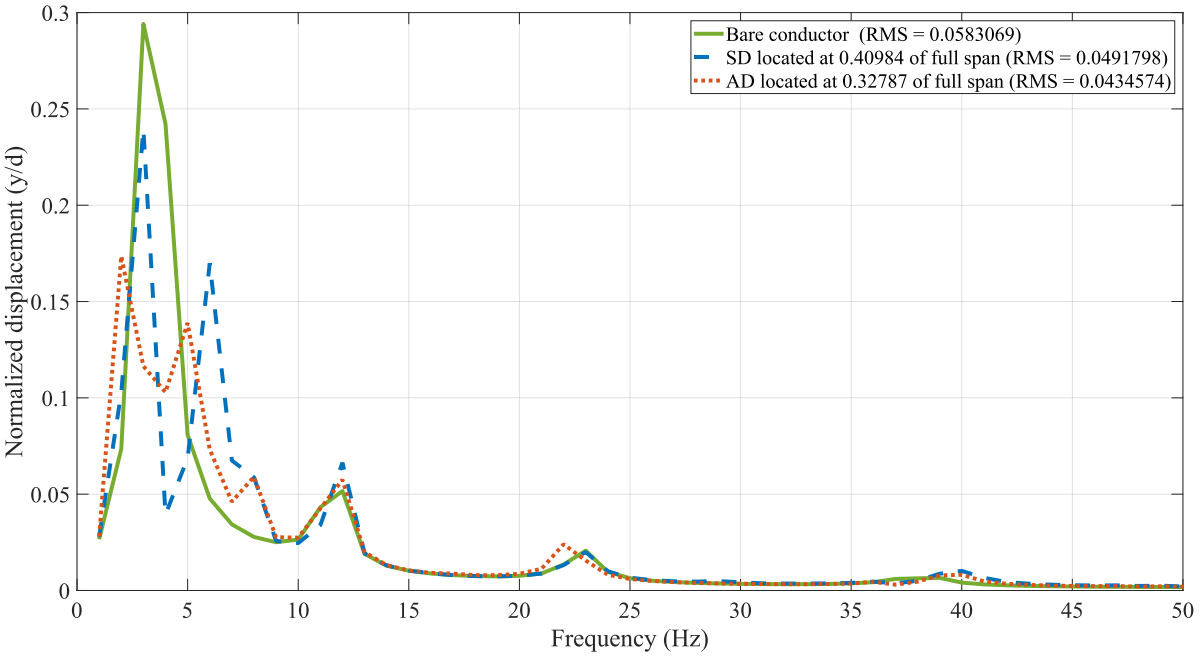

Fig. 5. Displacement responses of bare conductor, conductor with symmetrical and asymmetrical damper.

function, we can observe from Fig. 4 that the normalized optimal location of the symmetrical conductor is 0.40984, while the normalized optimal location of the asymmetrical damper is 0.32787. For completeness, we also compare the damper's performance using the conventional placement method, where the damper is positioned at 5 % to 10 % of the total length of the conductor from the pole. As shown in Fig. 4, at 10 % of the total conductor length, the normalized maximum displacement values for the symmetrical and asymmetrical dampers are 0.06014 and 0.05363, respectively. These values are notably higher than the displacements observed at the optimized placement positions. Thus, the optimized damper placements offer superior vibration reduction, demonstrating their effectiveness over the conventional placement method.

Next, Fig. 5 demonstrates the effectiveness of the dampers at their optimal locations by showing the RMS values of the system's response across different frequency components within the 0–50 Hz range. From Fig. 5, we can observe an average vibration reduction of approximately 15.65 % and 25.46 % by using the symmetrical and asymmetrical dampers in their respective optimal locations from Fig. 4. Notably, from Fig. 5, we can observe that the dampers are most effective in the frequency range of 0–5 Hz, which can be attributed to the first vibration mode of the system. However, as the excitation frequency increases beyond 5 Hz, their efficacy diminishes, leading to a noticeable rise in amplitude compared to the bare conductor's response. This observation suggests that these optimal damper locations are ideally suited for passive absorber design, particularly when dealing with excitation frequencies in the 0–50 Hz range, and especially within the first mode excitation of the conductor (2–5 Hz).

Finally, we determine the optimal location of the damper for each frequency component within the range of 0–50 Hz by minimizing the maximum displacement of the conductor. Fig. 6 illustrates the normalized damper location and the corresponding normalized maximum displacement of the conductor, presented on a log scale. We observe an overall vibration reduction of 53.29 % with asymmetrical dampers when placed at their respective optimal locations for the given frequency component. Conversely, a symmetrical damper results in a vibration reduction of 36.86 %, as indicated by the RMS values. This observation can be further attributed to the fact that asymmetrical Stockbridge dampers resonate at multiple natural frequencies due to their uneven mass and length distribution in comparison to the symmetrical Stockbridge dampers. This multi-frequency capability enhances their adaptability to varying environmental conditions and conductor loads. Their ability to engage in complex oscillatory modes, including both translational and rotational movements, facilitates more efficient energy dissipation from the conductor.

4. Experimental application

After establishing the superior performance of the asymmetrical damper compared to the symmetrical damper, we next develop the FE model for the commercially available asymmetrical damper to determine the optimum location. In order to determine the optimal location for the damper, we utilized the AMG-030513 Stockbridge damper, which is manufactured by Saprem. The experimental setup for the system is shown in Fig. 7. To establish the FE model of the AMG-030513 Stockbridge damper experimentally, we require the natural frequencies and actual mode shapes. For this purpose, we identify 29 points on the damper and capture the mode shapes using the laser vibrometer (Polytec PSV-500). To measure base excitation, an accelerometer, PCB Piezotronics 352C33, is mounted at the

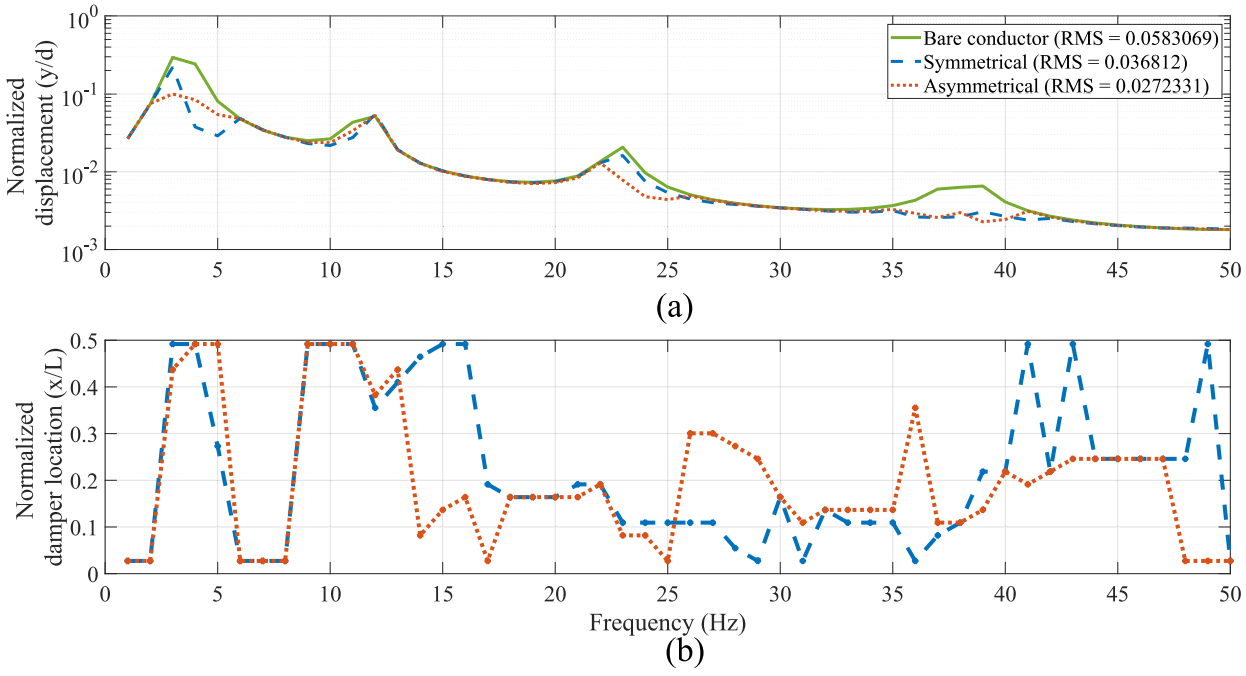

Fig. 6. (a) Normalized displacement for the optimal locations of damper corresponding to each frequency component, and (b) normalized optimal location of damper for each frequency component.

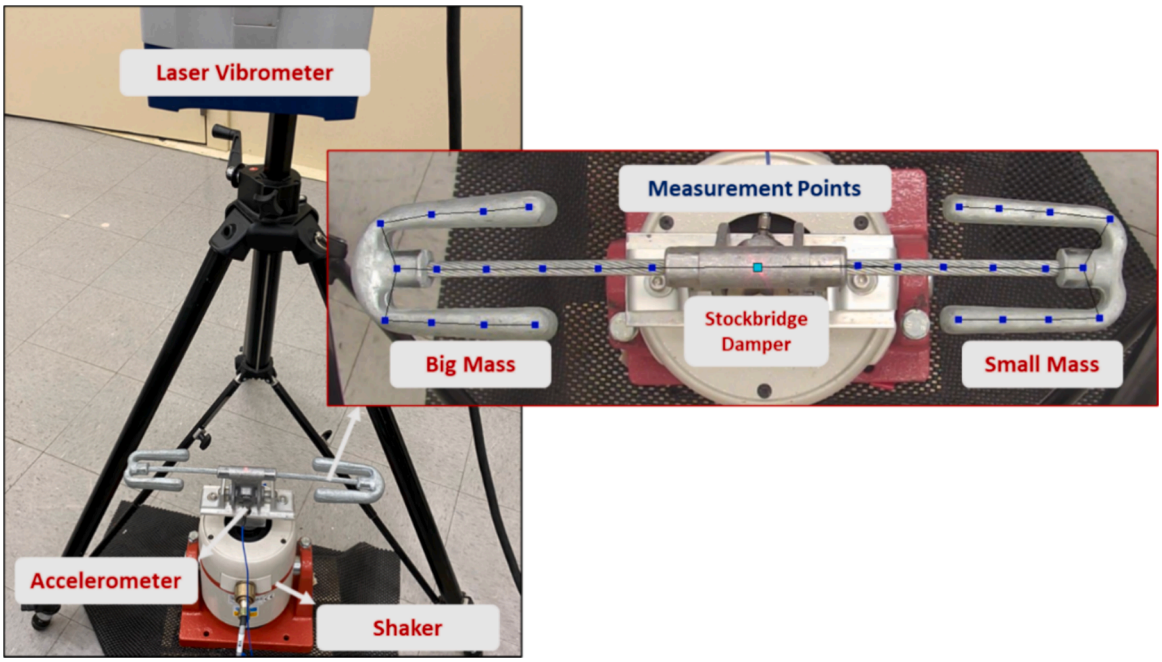

Fig. 7. Experimental setup for Stockbridge damper.

lower part of the damper connection fixture, as shown in Fig. 7. The system is excited using the LDS Test and Measurement V408 electrodynamic shaker. Furthermore, a signal conditioner, Polytec PSV-500, is used to acquire frequency responses of all the identified points and enable us to perform postprocessing on the obtained data.

We use two different excitations in our system: the burst random signal and the sine sweep signal. Contrary to the sine sweep test, the burst random test combines the advantages of both pure random and pseudo-random excitation, producing leakage-free signals that improve the accuracy of Frequency Response Functions (FRFs). A pseudo-random signal is applied in bursts, followed by rest periods where the system vibrates freely, allowing the response to decay within the sampling window. This ensures that the signals are fully contained and free from leakage artifacts. To ensure repeatability and accuracy of the results, we repeat the measurement nine times for each point using both signals. Accordingly, the resulting FRF is achieved by averaging the FRFs for each case. This averaging process further guarantees the acquisition of high-quality FRFs.

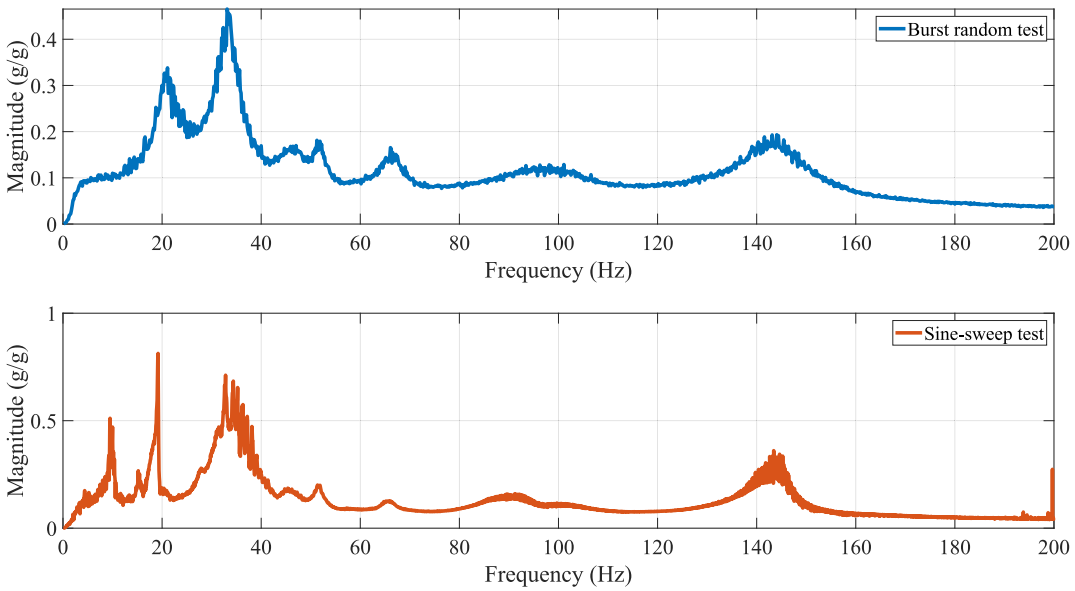

Fig. 8. Average frequency response functions of tests.

In the burst random test, a low-amplitude signal is applied for a duration of 6.4 s, starting at 5% intensity and with a burst length of 80%. To enhance the accuracy and consistency of the measurements, a rectangle windowing technique is employed. For the sine sweep test, a low amplitude signal ranging from 15 Hz to 200 Hz is used over 16 s. For the sine sweep test, a signal ranging from 15 Hz to 200 Hz over 16 s revealed that faster sweep rates are essential for capturing dynamic responses effectively, particularly in identifying resonant frequencies in systems with rapid dynamics. Slower sweep rates failed to produce satisfactory results, likely due to their inability to adequately capture rapid transient responses. Therefore, the fast sine sweep test for the period of 16 s has been utilized for the remainder of the analysis. A Hanning windowing method is also employed to enhance the quality of the data collected. Both tests utilize a sampling rate of 1250 Hz, chosen to ensure sufficient resolution and fidelity across a frequency range of 200 Hz. These parameters were carefully selected to accurately capture the relevant dynamics and characteristics of the damper, balancing the need for detailed frequency response with the practical limitations of testing speed and system behavior.

Fig. 8 depicts the average FRFs obtained from both the burst random and sine-sweep tests for all measurement points. From Fig. 8, we observe that the FRF from the burst random test exhibits more well-defined peaks compared to the FRF obtained from the sine sweep tests. Consequently, it is easier to identify the natural frequencies of the damper using the burst random test, making it a more reliable method for determining the underlying dynamics of the damper in this analysis.

The experimental mode shapes at the resonant frequencies (peak points of the FRFs) are shown in Fig. 9. These mode shapes are classified into two types: bending modes and torsional modes. It is important to note that the torsional modes of the damper do not significantly contribute to reducing vibrations in the conductor. On the other hand, the bending modes play a crucial role in achieving the desired vibration reduction in the conductor for the given frequency. Therefore, we only focus on the bending modes of the absorber to get effective vibration mitigation in the system. The mode shapes obtained from both signals, the burst random signal and the sine-sweep signal, exhibit remarkable similarities and match well with the existing literature [34]. This observation further validates the accuracy of the method employed for capturing the structural dynamics accurately.

Upon analyzing the obtained mode shapes in conjunction with the FRF, we observe that a rigid body motion occurs at 21 Hz. This motion can be attributed to a gap along the lateral axis of the shaker, which causes the damper to exhibit a peak point when excited at that frequency. As rigid body motion does not contribute to vibration mitigation, it has been excluded from the analysis. Furthermore, a distinct peak is observed at 10 Hz in the FRF corresponding to the sine-sweep test, which is not associated with any structural mode. This peak is likely a result of the initial excitation of the shaker. Since this peak can lead to misleading results, it is necessary to examine the mode shapes before the thorough analysis.

Next, we tune the commercial damper's FE model to conduct real-life analyses and determine the optimal damper location. A simplified FE model of the damper was constructed using the methodology mentioned earlier, ensuring that it exhibits similar natural frequencies and mode shapes as obtained experimentally. Again, the line bodies are used in the FE model to reduce computational time while maintaining accuracy. The schematic representations of the Saprem Stockbridge damper model, the finite element model, and the corresponding mesh model are shown in Fig. 10.

For the FE analysis, the damper was divided into 219 elements. Additionally, point masses are attached to the center of gravity to accurately represent the geometry of the counterweight in the actual damper. The finite element model is fixed from clamp ends to the ground, while the damper messengers are connected to the T-shaped clamp through fixed joints. Furthermore, the clamp is modeled as a rigid body to simulate realistic behavior, enhancing the overall accuracy of the simulation.

While the manufacturer provides some properties of the damper, essential properties, including the mass moment of inertia, counterweight's center of gravity, and messenger weight, are fine-tuned through trial and error to match the experimental values. This step ensures that a realistic FE model is employed for the analysis. The defined-measured and tuned parameters of the commercial damper are presented in Table 5. Note that the total damper mass from the manufacturer is stated as 1250 g in the datasheet; however, it was found to be approximately 1200 g when measured. Therefore, to match the actual damper weight, the mass of the messenger ($m_{messenger}$) is tuned to 0.25 kg/m. Additionally, rotational mass inertia properties are determined around the z-axis (which controls bending modes) and the x-axis (which governs torsional modes). The clamp material is an Aluminum alloy with Young's modulus of 71 GPa, Poisson's ratio of 0.33, and a mass density of 2,710 kg/m^3. Conversely, the messenger is Steel with Young's modulus of 200 GPa, and Poisson's ratio of 0.3.

To validate the tuned FE model of the damper, a free vibration analysis is performed to determine its natural frequencies. The comparison between the FE and experimental results is presented in Table 6. From Table 6, we can observe that the tuned FE model aligns very well with the results obtained from the burst random test, indicating a higher level of compatibility between the FE model and the burst random test. Therefore, it can be concluded that the burst random test yields the most accurate results when considering the finite element analysis.

Once the tuned FE model of the damper is validated, we use it in the experimentally verified FE model of the conductor to evaluate the dynamic response of the conductor within a specified frequency range. For this, we use the exact boundary condition and analysis as in Section 3.2, except for the loading configuration. In this case, a forcing amplitude ranging from 1 to 100 N is used, and the maximum deformation is computed for each damper location (as mentioned in Section 3.2) within the frequency range of 0–50 Hz. Further, the optimal location of the damper is obtained by determining the location which minimizes the maximum deformation for the given frequency. The frequency response and the optimal damper location for each frequency component are shown in Fig. 11. From Fig. 11, we can observe that an overall vibration reduction rate of 57.66 % can be achieved by strategically placing the commercial damper at the optimal locations for each frequency. This observation highlights the effectiveness of the proposed approach in mitigating vibrations in the conductor.

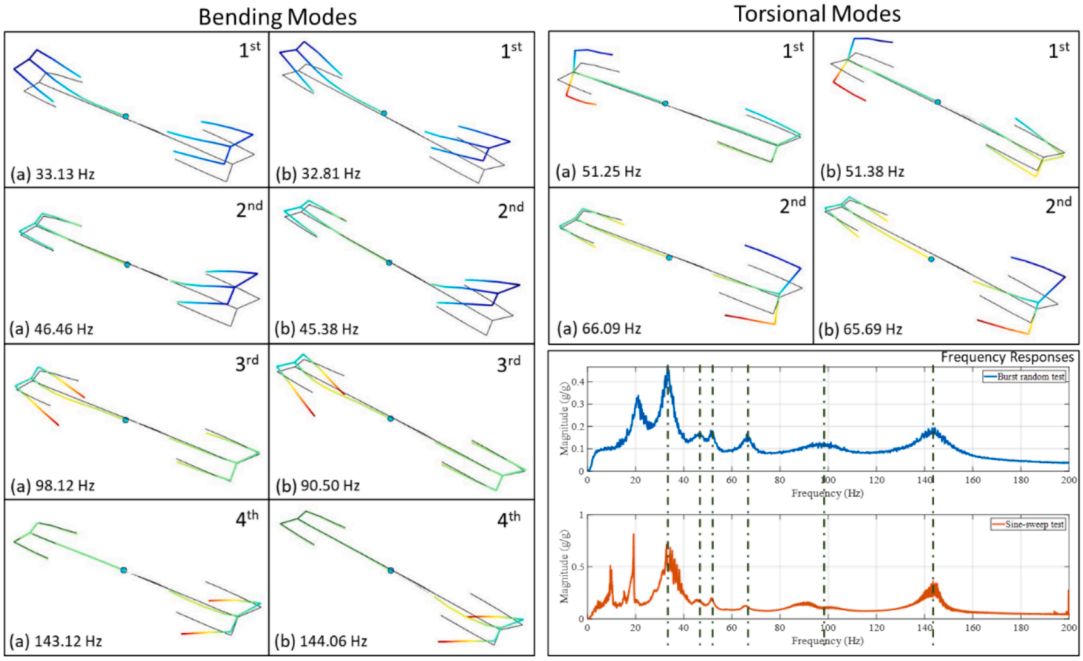

Fig. 9. Experimental mode shapes of (a) burst random (b) sine-sweep test.

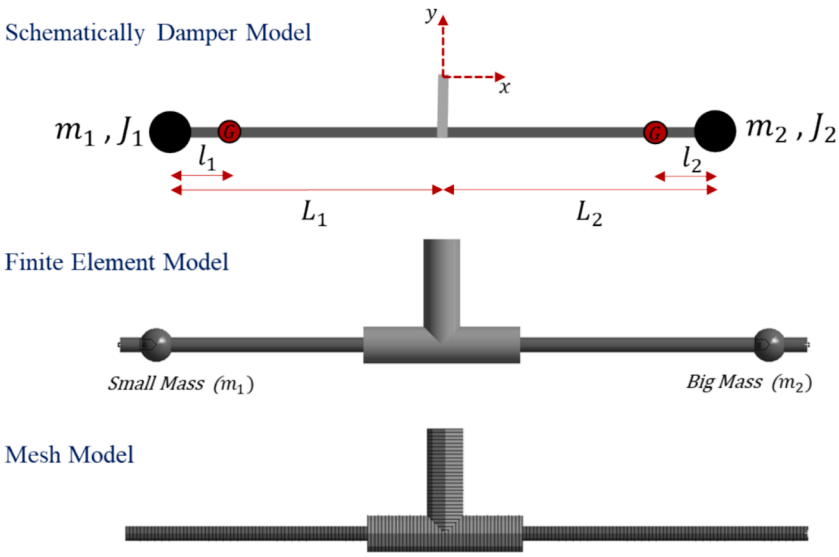

Fig. 10. Schematically, finite element and mesh model of the damper.

Table 5
The defined-measured and tuned parameters of Saprem AMG-030513.

Defined-Measured		*Tuned*	
$m_1(kg)$	*0.3*	$J_{1_z}(kg/mm^2)$	*2500*
$m_2(kg)$	*0.5*	$J_{2_z}(kg/mm^2)$	*1300*
$L_1(mm)$	*135*	$J_{1_x}(kg/mm^2)$	*3500*
$L_2(mm)$	*160*	$J_{2_x}(kg/mm^2)$	*1800*
$E(GPa)$	*200*	$l_1(mm)$	*17*
$d_{messenger}(mm)$	*8*	$l_2(mm)$	*21*
		$m_{messenger}(kg/m)$	*0.25*

Table 6
Experimental and finite element analysis results.

	No	Burst Random Test [Hz]	Sine-sweep Test [Hz]	FEA [Hz]	Mode
Bending Modes (on the z-axis)	***1st***	*33.13*	*32.81*	*33.75*	*Big mass first mode*
	2nd	*46.40*	*45.38*	*47.16*	*Small mass first mode*
	3rd	*98.12*	*90.50*	*97.98*	*Big mass second mode*
	4th	*143.12*	*144.06*	*147.76*	*Small mass second mode*
Torsional Modes (on the x-axis)	***1st***	*51.25*	*51.38*	*52.43*	*Big mass torsional mode*
	2nd	*66.09*	*65.69*	*66.99*	*Small mass torsional mode*

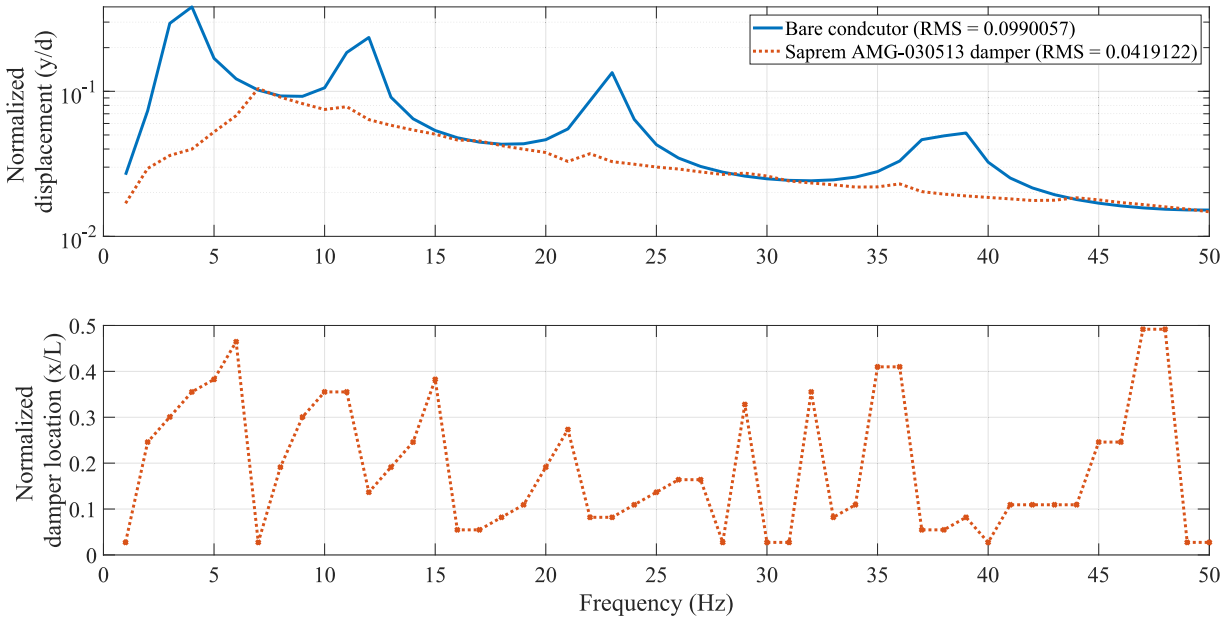

Fig. 11. Displacement responses against best damper location for Saprem damper.

5. Conclusions

This paper aimed to determine the optimal location of the Stockbridge damper in powerline conductors to enhance vibration mitigation. By employing finite element modeling, we successfully modeled both symmetrical and asymmetrical Stockbridge dampers along with the powerline conductor. The use of finite element models provided a more efficient and realistic representation of the damper-conductor system compared to traditional numerical methods. These models were validated against both experimental and numerical results, showing good agreement with the literature.

A key novelty of this study lies in the application of the burst random test, which proved to be more accurate and reliable than the conventional sine-sweep test in determining the natural frequencies and mode shapes of the Stockbridge dampers. This is the first time the burst random test has been used for this purpose in the context of Stockbridge dampers, demonstrating its superior ability to capture the dampers' dynamic behavior. The validated finite element models, combined with the experimental results, allowed us to identify optimal damper placements that significantly reduce aeolian vibrations.

The findings revealed that placing the damper at the optimized locations, identified through our proposed methodology, leads to a 53.29 % reduction in vibration for the asymmetrical damper, significantly outperforming conventional placement methods. This optimized placement strategy, validated through both simulation and experiments, has practical implications for improving the performance and longevity of powerline systems.

In conclusion, this study introduces novel experimental and computational approaches for analyzing and optimizing Stockbridge dampers. The insights gained from this research can help power companies and engineers design more effective and efficient powerline systems, ultimately benefiting infrastructure durability and reducing maintenance costs for consumers and society as a whole.

CRediT authorship contribution statement

Erdi Gulbahce: Writing – original draft, Software, Methodology, Investigation, Formal analysis, Conceptualization. **Sunit K. Gupta:** Writing – review & editing, Writing – original draft, Visualization, Investigation, Formal analysis, Conceptualization. **Oumar Barry:** Writing – review & editing, Visualization, Supervision, Resources, Project administration, Funding acquisition,

Conceptualization.

Declaration of competing interest

The authors declare the following financial interests/personal relationships which may be considered as potential competing interests: Oumar Barry reports financial support was provided by National Science Foundation. If there are other authors, they declare that they have no known competing financial interests or personal relationships that could have appeared to influence the work reported in this paper.

Acknowledgment

This work is partly supported by the National Science Foundation (NSF) Grant ECCS-1944032: CAREER: Towards a Self-Powered Autonomous Robot for Intelligent Power Lines Vibration Control and Monitoring.

Data availability

Data will be made available on request.

References

[1] R. Barbieri, N. Barbieri, O.H. de Souza Junior, Dynamical analysis of transmission line cables. Part 3—Nonlinear theory, *Mech. Syst. Sig. Process.* 22 (4) (2008) 992–1007.
[2] N. Barbieri, M.K.T. Calado, M.J. Mannala, K.F. de Lima, G.d.S.A.V. Barbieri, Dynamical analysis of various transmission line cables, *Procedia Eng.* 199 (2017) 516–521.
[3] K. Spak, G. Agnes, D. Inman, Cable modeling and internal damping developments, Appl. Mech. Rev. 65 (1) (2013).
[4] N. Barbieri, O.H. de Souza Júnior, R. Barbieri, Dynamical analysis of transmission line cables. Part 2—damping estimation, *Mech. Syst. Sig. Process.* 18 (3) (2004) 671–681.
[5] N. Barbieri, O.H. de Souza Júnior, R. Barbieri, Dynamical analysis of transmission line cables. Part 1—linear theory, *Mech. Syst. Sig. Process.* 18 (3) (2004) 659–669.
[6] J. Chan *et al.*, "EPRI Transmission Line Reference Book: wind-induced Conductor Motion," *EPRI, N° 1018554,* 2009.
[7] O.R. Barry, *Vibration Modeling and Analysis of a Single Conductor With Stockbridge Dampers*, University of Toronto, Canada, 2014.
[8] O. Barry, D.C. Oguamanam, D.C. Lin, Aeolian vibration of a single conductor with a Stockbridge damper, *Proc. Inst. Mech. Eng. C J. Mech. Eng. Sci.* 227 (5) (2013) 935–945.
[9] P. Kakou, M. Bukhari, J. Wang, O. Barry, On the vibration suppression of power lines using mobile damping robots, *Eng. Struct.* 239 (2021) 112312.
[10] O. Barry, J. Zu, D. Oguamanam, Analytical and experimental investigation of overhead transmission line vibration, *J. Vib. Control* 21 (14) (2015) 2825–2837.
[11] J. Sun, M. a. Jolly, M. t. Norris, "Passive, adaptive and active tuned vibration absorbers—a survey," 1995.
[12] N. Jalili, A comparative study and analysis of semi-active vibration-control systems, *J. Vib. Acoust.* 124 (4) (2002) 593–605.
[13] R. Herzog, Active versus passive vibration absorbers, *Trans.-Am. Soc. Mech. Eng. J. Dyn. Syst. Measure. Control* 116 (1994) 367.
[14] J. Morison, D. Karnopp, "Comparison of optimized active and passive vibration absorbers," in *Joint automatic control conference*, (11) 1973 932-938.
[15] N. Vaja, O. Barry, E. Tanbour, On the modeling and analysis of a vibration absorber for overhead powerlines with multiple resonant frequencies, *Eng. Struct.* 175 (2018) 711–720.
[16] M. Lu, J. Chan, An efficient algorithm for Aeolian vibration of single conductor with multiple dampers, *IEEE Trans. Power Delivery* 22 (3) (2007) 1822–1829.
[17] Z. Zondi, M. Kaunda, T. Ngonda, "Characteristics of the asymmetric Stockbridge damper," in *MATEC Web of Conferences*, 2021, vol. 347, p. 00005: EDP Sciences.
[18] N.K. Vaja, O. Barry, E.Y. Tanbour, "On the dynamic modeling and analysis of an asymmetric Stockbridge damper," in *Insights and Innovations in Structural Engineering, Mechanics and Computation*: CRC Press, 2016, pp. 71-75.
[19] O. Barry, J. Zu, D. Oguamanam, Nonlinear dynamics of Stockbridge dampers, *J. Dyn. Syst. Meas. Contr.* 137 (6) (2015) 061017.
[20] M.A. Bukhari, O. Barry, E. Tanbour, On the vibration analysis of power lines with moving dampers, *J. Vib. Control* 24 (18) (2018) 4096–4109.
[21] P.-C. Kakou, O. Barry, Toward a mobile robot for vibration control and inspection of power lines, *ASME Lett. Dyn. Syst. Control* 2 (1) (2022) 011001.
[22] N. Barbieri, R. Barbieri, R.A. da Silva, M.J. Mannala, L.d.S.A.V. Barbieri, Nonlinear dynamic analysis of wire-rope isolator and Stockbridge damper, *Nonlinear Dyn.* 86 (2016) 501–512.
[23] T. de Freitas Pinto, A.C. Araujo, C.F.T. Matt, Analytical, Numerical and Experimental Investigation of the Dynamic Behavior of A Prototype for A Stockbridge Damper. In *20th International Congress of Mechanical Engineering*, 2009.
[24] D. Sauter, P. Hagedorn, On the hysteresis of wire cables in Stockbridge dampers, *Int. J. Nonlinear Mech.* 37 (8) (2002) 1453–1459.
[25] E. Gülbahçe, M. Çelik, Experimental modal analysis for the plate structures with roving inertial shaker method approach, *J. Low-Frequency Noise Vib. Active Control* 41 (1) (2022) 27–40.
[26] J. Vecchiarelli, "Aeolian vibration of a conductor with a Stockbridge-type damper," 1998.
[27] ANSYS. (10.01.2023). *BEAM188 ELEMENT*. Available: https://www.mm.bme.hu/~gyebro/files/ans_help_v182/ans_elem/Hlp_E_BEAM188.html.
[28] C.-J. Kim, Design sensitivity analysis of a Stockbridge damper to control resonant frequencies, *J. Mech. Sci. Technol.* 31 (2017) 4145–4150.
[29] O. Barry, "Finite element analysis of a single conductor with a Stockbridge damper under Aeolian vibration'," *MASc, Mechanical Engineering, Ryerson University, Toronto, Canada,* 2010.
[30] R. Claren, G. Diana, Mathematical analysis of transmission line vibration, *IEEE Trans. Power Syst.* 12 (1969) 1741–1771.
[31] Ş. Yıldırım, E. Esim, "Harmonic response analysis of double bridge crane system on multi carriages," in *5th International Conference on Engineering and Naturel Science. Prague*, 2019, pp. 90-96.
[32] Z. Zeng, J. Li, S. Zhang, Y. Hong, Y. Wang, Analysis of the harmonic response of a modulation permanent magnetic transmission equipment based on ANSYS, *Energy Power Eng.* 7 (03) (2015) 63.
[33] Y. Yu, S. Zhang, H. Li, X. Wang, Y. Tang, Modal and harmonic response analysis of key components of ditch device based on ANSYS, *Procedia Eng.* 174 (2017) 956–964.
[34] X. Luo, L. Wang, Y. Zhang, Nonlinear numerical model with contact for Stockbridge vibration damper and experimental validation, *J. Vib. Control* 22 (5) (2016) 1217–1227.